

A Simple method to set up low eccentricity initial data for moving puncture simulations

Wolfgang Tichy and Pedro Marronetti

Department of Physics, Florida Atlantic University, Boca Raton, FL 33431, USA

We introduce two new eccentricity measures to analyze numerical simulations. Unlike earlier definitions these eccentricity measures do not involve any free parameters which makes them easy to use. We show how relatively inexpensive grid setups can be used to estimate the eccentricity during the early inspiral phase. Furthermore, we compare standard puncture data and post-Newtonian data in ADMTT gauge. We find that both use different coordinates. Thus low eccentricity initial momentum parameters for a certain separation measured in ADMTT coordinates are hard to use in puncture data, because it is not known how the separation in puncture coordinates is related to the separation in ADMTT coordinates. As a remedy we provide a simple approach which allows us to iterate the momentum parameters until our numerical simulations result in acceptably low eccentricities.

PACS numbers: 04.25.dg, 04.25.Nx, 04.20.Ex, 04.30.Db,

I. INTRODUCTION

Currently several gravitational wave detectors such as LIGO [1, 2], Virgo [3, 4] or GEO [5] are already operating, while several others are in the planning or construction phase [6]. One of the most promising sources for these detectors are the inspirals and mergers of binary black holes. In order to make predictions about the final phase of such inspirals and mergers, fully non-linear numerical simulations of the Einstein Equations are required. To numerically evolve the Einstein equations, at least two ingredients are necessary. First we need a specific formulation of the evolution equations. And second, to start such simulations initial data are needed. As the first ingredient most groups nowadays use the BSSNOK formulation [7–9] of the evolution equations. This formulation is usually evolved using finite differencing methods, but for single black holes there have been some attempts to use spectral methods [10–12]. For binary black holes the BSSNOK system is usually used together with the moving puncture approach [13, 14]. This approach so far works only with finite differencing methods since certain evolved variables are not smooth inside the black holes (at the punctures). Almost all simulations using the BSSNOK formulation to date use standard puncture data [15, 16] as initial data. These initial data are very flexible in that they contain free parameters for the position, momentum and spin of each black hole and thus one can setup practically any kind of orbit. Note, however, that the emission of gravitational waves tends to circularize the orbits [17, 18]. Thus for realistic binary black hole systems that have been inspiraling already for a long time, we expect the two black holes to be in quasi-circular orbits around each other with a radius which shrinks on a timescale much larger than the orbital timescale. This means that the initial data should be such that the orbit has no or at least very small eccentricity. For our purposes here we follow the NRAR (Numerical Relativity - Analytical Relativity) collaboration [19] guidelines

which consider eccentricities of order a few times 10^{-3} acceptably small. There have been several previous works that have considered eccentricities for puncture initial data [20–22]. However, the most successful approach in terms of achieving low eccentricities was implemented for excision type initial data [23–25]. The method discussed in this work aims at lowering the eccentricity for the kind of puncture initial data that is routinely used with the moving puncture approach.

Throughout we will use units where $G = c = 1$. The black hole masses are denoted by m_1 and m_2 . We also introduce the total mass $M = m_1 + m_2$, the reduced mass $\mu = m_1 m_2 / M$ and $\nu = \mu / M$.

The paper is organized as follows. Sec. II introduces and compares several eccentricity measures. In Sec. III we describe grid setups that can be used in numerical simulations aimed at measuring the eccentricity. Sec. IV discusses a simple method to pick initial momentum parameters. This is followed by Sec. V which describes how to iterate these parameters to arrive at a reduced eccentricity. We conclude with a discussion of our results in Sec. VI.

II. DEFINING ECCENTRICITY FOR INSPIRAL ORBITS

Real binary black hole orbits can never be circular. They always follow spirals. So when we are aiming for low eccentricity initial data, we really want data that result in trajectories that spiral in smoothly without oscillations in the black hole separation. Of course this issue is further complicated by the fact that trajectories are coordinate dependent.

There are several earlier eccentricity definitions for inspiral orbits in the literature [20–25]. All of them define eccentricity as a deviation from an underlying smooth, secular trend in some specific quantity that is associated with the orbits. In [20] the frequency of the dominant $l = m = 2$ mode of the gravitational waves emitted is fit-

ted to a fourth order monotonic polynomial, and the deviation of the frequency from this fit is used to compute the eccentricity. This approach works for non-spinning binaries. Essentially the same method is also used in [21], but instead of the gravitational wave frequency [21] uses the orbital frequency and also the coordinate separation to obtain two eccentricity measures. These same measures are also used in [22]. The approaches in [23, 24] fit a linear function plus a sine function to the coordinate separation and also the proper separation. The eccentricity can then be obtained from the amplitude of the fitted sine function. In [25] the same fitting approach as in [21] is used, but the fitted quantities are coordinate separation, proper separation and also orbital frequency. All the approaches based in orbital parameters should in principle also work for systems with spin. Also note that all these eccentricity definitions are chosen such that they result in the correct value for Newtonian orbits.

Below we will introduce two new eccentricity definitions and compare them to the earlier definition based on fitting the orbital frequency [21, 25].

The first eccentricity definition is based on the coordinate separation of the two black holes. It is given by

$$e_r(t) = \frac{\Delta r_{max}(t) - \Delta r_{min}(t)}{2r_{av}} \quad (1)$$

where the average separation, and the maximum and minimum deviation from a smoothed value r_s are given by

$$r_{av} = \int_{t-T/2}^{t+T/2} r(t') dt' / T \quad (2)$$

$$\Delta r_{max}(t) = \max_{t' \in [t-T/2, t+T/2]} [r(t') - r_s(t', t)] \quad (3)$$

$$\Delta r_{min}(t) = \min_{t' \in [t-T/2, t+T/2]} [r(t') - r_s(t', t)]. \quad (4)$$

Here the period T is defined using Kepler's law

$$T = 2\pi(r^3/M)^{1/2}. \quad (5)$$

Notice that the actual orbital period may be slightly different, but this estimate suffices to get an approximate eccentricity measure. The smoothed value $r_s(t', t)$ is obtained from

$$r_s(t', t) = r(t) + \frac{r(t+T/2) - r(t-T/2)}{T}(t' - t), \quad (6)$$

but different smoothings are possible (e.g., by performing a least-squares fit of e.g. a linear or quadratic function to $r(t)$ in the interval $[t+T/2, t-T/2]$). Essentially the definition in Eq. (1) measures how much the coordinate separation oscillates over the time T . For Newtonian orbits it coincides with the usual eccentricity definition for elliptic orbits. For orbits whose radius shrinks linearly in time (without any oscillations) $e_r(t)$ is zero.

Another similar eccentricity measure can be obtained using the gravitational wave signal of the inspiraling

binary. The idea is to determine the separation in a more gauge invariant way from the amplitude of Ψ_4 instead of using the gauge dependent coordinate separation. In [26] it is shown that for a non-precessing binary in the quadrupole approximation the amplitude of the $l = m = 2$ spin-weighted Spherical Harmonic mode is given by

$$|C_{22}| = 32\sqrt{\pi/5}\nu(M\omega)^{8/3}, \quad (7)$$

where ω is the orbital angular velocity. Using Kepler's law we can define a separation

$$r_{22} = M^{1/3}\omega^{-2/3} = M[|C_{22}|/(32\sqrt{\pi/5}\nu)]^{-1/4} \quad (8)$$

which is directly related to the amplitude of $|C_{22}|$ of the $l = m = 2$ mode of Ψ_4 . Replacing the coordinate separation in Eq. (1) by r_{22} we define

$$e_{22}(t) = \frac{\Delta r_{22,max}(t) - \Delta r_{22,min}(t)}{2r_{22,av}}, \quad (9)$$

which is an eccentricity definition that can be computed from Ψ_4 alone. Note that this definition needs to be extended for the case of precessing orbits, since in that case $|C_{22}|$ will oscillate even for spherical orbits (i.e. orbits with $r = \text{const}$). The extension could be achieved by instead using a $|C_{22}|$ that is computed in a coordinate system where the z-axis points along the instantaneous orbital angular momentum.

We have also tested an eccentricity definition based on the coordinate angular velocity ω . Here the eccentricity is defined by [21, 25]

$$e_\omega(t) = \frac{\omega(t) - \omega_{fit}(t)}{2\omega_{fit}(t)}, \quad (10)$$

where $\omega(t)$ is simply the coordinate angular velocity and $\omega_{fit}(t)$ is a polynomial fit of order 5 to $\omega(t)$ over a time interval corresponding to several complete orbits. The hope is that the fit will smooth out oscillations so that $e_\omega(t) \propto \omega(t) - \omega_{fit}(t)$ becomes a measure of how much ω oscillates. The actual eccentricity is the maximum magnitude of $e_\omega(t)$.

In order to compare these three eccentricity definitions we now present the eccentricities from an actual numerical simulation. As we can see in Fig. 1 all three eccentricity definitions agree well for $300M \leq t \leq 3000M$. They yield a value of about 0.02. Notice that e_r and e_{22} are direct eccentricity measures, while in the case of e_ω the eccentricity corresponds to the maximum value of the magnitude of e_ω . The eccentricity definition e_r which is calculated from the separation has certain problems for $t < T/2 \sim 135M$. These occur because we have no data for $t < 0$, which is needed in the average over one complete period (centered around t) and also for the fitting in Eq. (6). These same problems also affect e_{22} . In e_{22} , however, they are exacerbated by the initial junk radiation that dominates $|C_{22}|$ until about $150M$ (see middle panel). We see that e_{22} does not completely settle

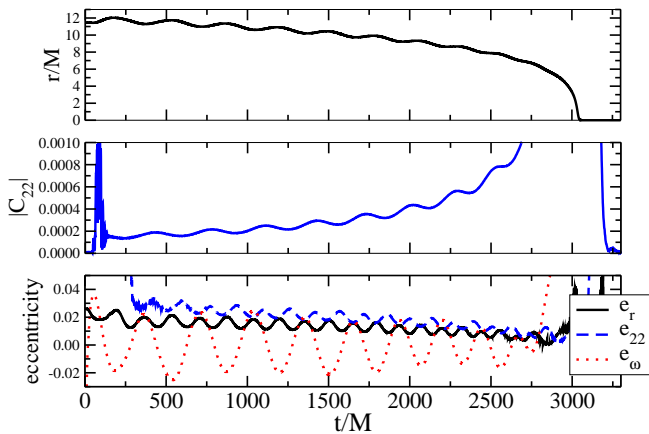


FIG. 1: This plot shows results from a numerical run (with parameters from row 6 of table I. The upper panel shows the coordinate separation r . The middle panel depicts the magnitude of the $l = m = 2$ mode $|C_{22}|$ of Ψ_4 extracted at a separation of $70M$ from the center of mass. In the lower panel we plot the three different eccentricities obtained with the definitions given in Eqs. (1), (9) and (10). Note that e_r and e_r directly measure eccentricity, while for e_ω the eccentricity corresponds to the maximum values of $|e_\omega(t)|$.

down until about $700M$. Notice also that during standard moving puncture evolutions the coordinates adjust quite rapidly initially. This means that any eccentricity definition that is based on the coordinate separation or the coordinate angular velocity will not be completely reliable during the first $100M$ or so. Thus it comes as no surprise that the eccentricity definition e_ω has a different frequency and amplitude in the beginning.

The curves for e_r and e_{22} in Fig. 1 oscillate even at later times. This oscillation is due to the fact that the period T which we get from Kepler's law is not exactly equal to the actual orbital period. The magnitude of this oscillation can be used as an error estimate of our eccentricity measures. For a conservative eccentricity estimate we can use the maximum values of e_r and e_{22} .

Let us point out that e_r and e_{22} are easier to compute than e_ω . The latter depends on a polynomial fit to the measured orbital angular velocity. The problem is that this fit has to be done over a certain time interval, that must terminate well before the merger. Thus it requires a certain amount of fine tuning and human intervention. On the other hand e_r and e_{22} can be computed at any time in a very simple way. Recall however, that e_{22} is more sensitive to the initial junk radiation. Thus for short runs used to probe the eccentricity of a configuration we usually just use e_r .

III. NUMERICAL EVOLUTIONS

The numerical results discussed in this paper have been obtained with the BAM code [27–29]. As already mentioned, the gravitational fields are evolved using the BSS-

NOK formalism [7–9] in the variation known as the “moving punctures” method [13, 14]. The particulars of our BSSNOK implementation can be found in [28, 29]. For completeness we note that lapse and shift evolve according to

$$\begin{aligned} (\partial_t - \beta^i \partial_i) \alpha &= -2\alpha K, \\ (\partial_t - \beta^k \partial_k) \beta^i &= \frac{3}{4} B^i, \\ (\partial_t - \beta^k \partial_k) B^i &= (\partial_t - \beta^k \partial_k) \tilde{\Gamma}^i - \eta B^i. \end{aligned} \quad (11)$$

The shift driver parameter is set $\eta = 2/M$ in all our runs.

The BAM code is based on a method of lines approach using sixth order finite differencing in space and explicit fourth order Runge-Kutta time stepping. The time step size is chosen such that the Courant factor is either 0.25 or 0.5. For efficiency, Berger-Oliger type mesh refinement is used [30]. The numerical domain is represented by a hierarchy of nested Cartesian boxes. The hierarchy consists of $L + 1$ levels of refinement, indexed by $l = 0, \dots, L$. A refinement level consists of one or two Cartesian boxes with a constant grid-spacing $h_l = h_0/2^l$ on level l . We have used here $L = 10$ to 11 for the number of refinement levels, with the levels 0 through 5 each consisting of a single fixed box centered on the origin (the center of mass). On each of the finer levels 6 through L , we initially use two sets of moving boxes centered on each black hole. When the black holes get close enough that two of these boxes start touching, they are replaced by a single box. The position of each hole is tracked by integrating the shift vector. We use this same set up but with different resolutions depending on the purpose of each simulation.

For an accurate simulation of the inspiral and merger of two non-spinning equal mass black holes we might use $L = 10$ with a resolution $h_{10} = M/96$ on the finest level using 144 points on the fixed levels and 72 points on the moving levels. The notation we use to describe this grid setup for this simulation is:

$$[5 \times 72, 6 \times 144][M/h_{10} = 96, OB = 768M][C = 0.25] \quad (12)$$

which indicates that we have 5 moving levels with 72 points in each box and 6 fixed levels with 144 points each. The resolution is given by $M/h_{10} = 96$ on the finest level, which results in an outer boundary at $768M$. The Courant factor here is chosen to be 0.25, which implies a time step of $dt_{10} = 0.25h_{10} = M/384$ on the finest level. If the black holes have spins and/or unequal masses even more resolution is needed. For example for a mass ratio of 3 and a dimensionless spin magnitude of 0.6 on the larger hole we might use a setup described by:

$$[6 \times 72, 6 \times 144][M/h_{11} = 192, OB = 768M][C = 0.25] \quad (13)$$

this setup has twice the resolution on the finest level, so that the resolution in terms of the individual masses is now given by $m_1/h_{11} = 48$ for the smaller and $m_2/h_{11} = 144$ for the larger hole. Such runs are quite expensive.

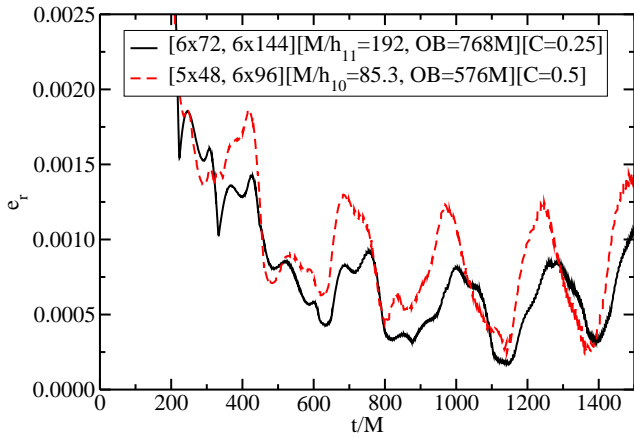


FIG. 2: This plot shows the eccentricity e_r for two different grid setups. Both start with the parameters from row 7 of table I. The solid line shows e_r for a high resolution grid, while the broken line shows the measured e_r if we use a less accurate and computer intensive grid setup. Both yield similar orbital eccentricities.

Until merger they take about one month on a Cray XT5 supercomputer like NICS Kraken if we use 96 cores.

However, if our objective is to simply measure the orbital eccentricity of a binary (characterized by certain initial parameters), it is sufficient to evolve for only a few orbits. We have found that such an evolution does not need great accuracy. So if the goal is to simply determine the initial eccentricity we use the following setup

$$[5 \times 48, 6 \times 96][M/h_{10} = 85.3, OB = 576M][C = 0.5] \quad (14)$$

With this grid setup it takes only two days to evolve up to $t = 800M$ if we use 48 cores on NICS Cray XT5 Kraken. In Fig. 2 we see that the eccentricity e_r from this cheaper run agrees quite well with the e_r from a more expensive run. As explained above no eccentricity estimate is accurate at the start of a run. We need to wait until about $500M$ for e_r to settle down to a regular oscillation. As mentioned before we use the maxima of e_r as a conservative eccentricity estimate. Thus the eccentricities of the cheap and expensive runs are 0.0013 and 0.0010. Hence we need to evolve until at least about $800M$ to get a reliable estimate. From the oscillations in the curves we see that the errors in both eccentricity estimates are about 0.0005.

IV. CHOOSING PUNCTURE PARAMETERS

In order to start our simulations we need initial data for binary black holes with arbitrary spins and masses at some given initial separation r . Since we will employ the moving punctures approach in our evolutions, we will use standard puncture initial data [15]. Thus the 3-metric and extrinsic curvature are given by

$$g_{ij} = \psi^4 \delta_{ij} \quad (15)$$

$$K^{ij} = \psi^{-10} \sum_{A=1}^2 \left\{ \frac{3}{r_A^2} \left[p_A^{(i} n_A^{j)} - \frac{\delta_{kl} p_A^k n_A^l}{2} (\delta^{ij} - n_A^i n_A^j) \right] + \frac{6}{r_A^2} \left[\epsilon_{klm} S_A^l n_A^m \delta^{k(i} n_A^{j)} \right] \right\}. \quad (16)$$

Here p_A^i and S_A^i are the momentum and spin parameters of black hole A , while r_A and n_A^i denote the distance and normal vector measured from hole A . The conformal factor is

$$\psi = 1 + \frac{m_{b1}}{2r_1} + \frac{m_{b2}}{2r_2} + u, \quad (17)$$

where m_{b1} and m_{b2} denote the black hole bare mass parameters. The scalar u is computed by numerically solving the Hamiltonian constraint. These initial data are very flexible since the free parameters for the position, momentum and spin of each black hole can be chosen freely. Thus one can setup practically any kind of orbit. Note, however, that our goal is to set up data for black holes that are in quasi-circular orbit. This means that we need to choose our momentum parameters such that the eccentricity is as small as possible. Since we start our evolutions in a frame where the center of mass is at rest, both black holes have momenta that are equal in magnitude but opposite in direction. Thus we have to choose only two parameters: the tangential and radial component of the momentum of one of the black holes.

To complete the definition of the initial data, we also need to specify initial values for the lapse α and shift vector β^i . At time $t = 0$ we use

$$\alpha = \psi^{-2}, \quad \beta^i = 0. \quad (18)$$

A. Finding the momentum parameters

There have been various attempts to guess appropriate momentum parameters. Some have used the quasi-equilibrium approach [31–33], but most are based on post-Newtonian (PN) approximations (see e.g. [29, 34, 35]). The latter have been taken to their extreme in [21] and [22] who integrate PN equations in the ADMTT gauge [36] in the hope that the thus obtained momentum parameters will lead to orbits with less eccentricity. However, as mentioned in [22], it is not certain that non-eccentric PN parameters in ADMTT gauge should produce non-eccentric orbits in full General Relativity. We want to point out here, that standard puncture data are inconsistent with PN theory beyond $(v/c)^3$ [46] [34, 37–39], even in ADMTT gauge! The reasons for this inconsistency are as follows. First, the 3-metric of puncture data is always conformally flat (see Eq.(15)), while the PN 3-metric contains deviations from conformal flatness at order $(v/c)^4$ [37, 40]. This is true for both harmonic and ADMTT gauge. Second, the conformal factor in

ADMTT gauge is given by [37]

$$\psi_{PN} = 1 + \frac{E_1}{2r_1} + \frac{E_2}{2r_2}, \quad (19)$$

where E_A is the energy of each particle used to model the black holes. If we compare Eqs. (19) and (17) we see that the conformal factor in ADMTT gauge is not identical to the conformal factor used in puncture initial data. One difference is that the ADMTT ψ_{PN} contains the particle energies E_A while the puncture ψ contains the bare masses m_{bA} . These two only agree for infinite separation. Furthermore, the puncture ψ contains the additional piece u that is obtained by numerically solving the Hamiltonian constraint, while PN data violates the Hamiltonian constraint. One might like to argue that the PN data should agree with puncture data up to the higher order terms that are neglected in the PN approximation. This is however not true close to the black holes, because PN theory is not valid in regions of very strong gravity. Thus near the black holes the ADMTT metric differs from the puncture metric by terms that are of low PN order.

From the above explanation it is clear that the coordinate separation in ADMTT gauge does not have the same physical meaning as the coordinate separation in puncture initial data. Thus if by some method we arrive at the momentum parameters needed at a particular separation r (in ADMTT coordinates), we should not simply use these same momentum parameters at the same puncture separation.

So if (for some configurations) the more complicated approaches in [21] or [22] lead to less eccentric orbits than e.g. the simpler approaches in [29, 34, 35] this should be considered a coincidence, since it is not due to the inclusion of higher order terms or due to the integration of post-Newtonian equations of motion. In fact, we find that (as anticipated by [22]) for many configurations the approaches in [21] or [22] do not lead to less eccentricity than the ones in [29, 34, 35].

For these reasons we take a different approach here. We will take a simple PN formula to obtain a reasonable guess for both the tangential and radial momentum components p_t and p_r . Then we numerically evolve the resulting initial data for a short time (using the efficient grid setup in Eq. (14)) to see how eccentric they really are. Afterward we adjust p_t to reduce the eccentricity. In this way we can obtain low eccentricity orbits for any configuration. In order to come up with a reasonable guess for p_t and p_r we use 2PN accurate expressions of Kidder [41] in harmonic gauge. Specifically, we freely choose the two masses m_1, m_2 , the six spin components of \mathbf{S}_1 and \mathbf{S}_2 and a separation r . Next, choosing $\hat{\mathbf{L}}_N$ in the z -direction, we use Eqs. (2.8) and (4.7) of [41] to compute the total orbital angular momentum \mathbf{L} , and Eq. (4.12) of [41] to compute \dot{r} . We rotate \mathbf{L} , \mathbf{S}_1 and \mathbf{S}_2 so that \mathbf{L} points in the z -direction. Then we obtain the momentum in the xy -plane as

$$p_t = |\mathbf{L}|/r \quad (20)$$

$$p_r = \mu|\dot{r}|. \quad (21)$$

In all cases discussed in this paper we put the two punctures on the y -axis at $y_1 = m_2 r/M$ and $y_2 = -m_1 r/M$. The two initial black hole momenta are then $\mathbf{p}_1 = (-p_t, -p_r, 0)$ and $\mathbf{p}_2 = (p_t, p_r, 0)$.

B. Determining the bare mass parameters

The momenta $\mathbf{p}_1, \mathbf{p}_2$ and the spins $\mathbf{S}_1, \mathbf{S}_2$ for a coordinate separation r directly enter the Bowen-York extrinsic curvature of standard puncture data. Note, however, that the bare mass parameters m_{b1} and m_{b2} which appear in the construction of standard puncture data are not equal to the individual black hole masses. As in [29, 34, 42, 43] we obtain the bare masses from the condition that the ADM masses

$$m_A^{ADM} = m_{bA}(1 + u_A) + \frac{m_{b1}m_{b2}}{2r}, \quad (22)$$

measured at the punctures [44] should be equal to m_1 and m_2 , where u_A is the value of u at puncture A . As in [16, 33, 44] we assume that the ADM masses measured at each puncture are a good approximation for the initial individual black hole masses. Numerically this condition is implemented as a root finder in the initial data solver that picks m_{b1} and m_{b2} such that the ADM masses at the punctures are equal to m_1 and m_2 .

V. REDUCING THE ECCENTRICITY

Now that we know how to generate initial data on approximately circular orbits for arbitrary spins, masses and separations, it is time to present some numerical results to demonstrate what eccentricities we get and how we can reduce them. For our purposes here, we consider the eccentricity small enough if it is 0.003 or less, which agrees with the NRAR target of an eccentricity of a few times 10^{-3} . The first example we consider is an equal mass binary without spin. The momentum parameters are picked according to Eqs. (20) and (21). The values of all the initial parameters are given in the first line of table I. As we can see, the eccentricity is about 0.005 in this case. In order to test how it varies with p_t we have also performed a run where we have increased p_t by

$$\Delta p_t = \mu\sqrt{\frac{M}{r}} \left[11.29 \left(\frac{M}{r} \right)^3 - 92.37 \left(\frac{M}{r} \right)^4 \right]. \quad (23)$$

The results of this increase are shown in the second line of table I and yield an eccentricity that is reduced by more than a factor of 3. The expression for Eq. (23) comes from the fitting of two of our older equal mass runs that resulted in low eccentricity. Thus non-zero spins or unequal masses are not taken into account by this fit. Therefore Eq. (23) certainly does not present the optimum momentum correction. In fact we have found that

row	$\frac{r}{M}$	$\frac{m_{b1}}{M}$	$\frac{m_{b2}}{M}$	$\frac{m_1}{M}$	$\frac{m_2}{M}$	$\frac{ \mathbf{S}_1 }{m_1^2}, \theta_1, \phi_1$	$\frac{ \mathbf{S}_2 }{m_2^2}, \theta_2, \phi_2$	$\frac{10^2 p_t}{M}$	$\frac{10^4 p_r}{M}$	$10^3 e_r$
1	11.9718	0.488255	0.488255	1/2	1/2	0	0	8.5018	3.88	5.0
2	11.9718	0.488249	0.488249	1/2	1/2	0	0	8.5168	3.88	1.5
3	11.9694	0.404597	0.404687	1/2	1/2	0.6, 60, 0	0.6, 120, 90	8.5013	3.87	4.0
4	11.9694	0.404592	0.404681	1/2	1/2	0.6, 60, 0	0.6, 120, 90	8.5163	3.87	2.0
5	11.9694	0.404588	0.404677	1/2	1/2	0.6, 60, 0	0.6, 120, 90	8.5280	3.87	1.5
6	11.4546	0.2239	0.6145	1/4	3/4	0.4, 0, 0	0.6, 0, 0	6.4416	2.21	20
7	10.7271	0.223341	0.614005	1/4	3/4	0.4, 0, 0	0.6, 0, 0	6.6396	2.50	1.0
8	12.0815	0.224174	0.614794	1/4	3/4	0.4, 180, 0	0.6, 180, 0	6.5900	2.50	1.0
9	11.7173	0.223891	0.614572	1/4	3/4	0.4, 180, 0	0.6, 180, 0	6.7497	4.08	5.0
10	10.9876	0.223317	0.614121	1/4	3/4	0.4, 0, 0	0.6, 180, 0	6.9756	3.19	3.0
11	11.5010	0.300017	0.543886	1/3	2/3	0.4, 60, 0	0.6, 60, 0	7.6504	3.18	2.0
12	11.5033	0.300020	0.543926	1/3	2/3	0.4, 60, 0	0.6, 60, 90	7.6509	3.19	1.8
13	11.6182	0.300023	0.543980	1/3	2/3	0.4, 60, 0	0.6, 120, 90	7.7896	3.51	2.1
14	11.5502	0.310095	0.656229	1/3	2/3	0.3, 0, 0	0	7.7196	3.32	1.3

TABLE I: Initial data parameters. The black holes have coordinate separation r . We give both bare masses m_{b1} , m_{b2} as well as physical masses m_1 , m_2 . The punctures are located on the y -axis at $y_1 = m_2 r/M$ and $y_2 = -m_1 r/M$. The spins are given in terms of their magnitudes and the usual polar angles of spherical coordinates measured in degrees. The linear momenta are $(\mp p_t, \mp p_r, 0)$. The last column shows the resulting eccentricity.

adding Δp_t to p_t does not always reduce the eccentricity since the PN estimate of Eq. (20) for p_t is sometimes too large and sometimes too small for generic orbits. The expression in Eq. (23) simply gives us a rough estimate by how much we might have to raise or lower p_t in order to reduce the eccentricity.

So in order to really reduce the eccentricity we usually start one run on the coarse grid described by Eq. (14). This run normally uses p_t given by Eq. (20). We then look at the coordinate separation $r(t)$ for this run. Usually one can tell whether the initial tangential momentum p_t was too large or too small. We then start a new run where we either increase or decrease p_t by Δp_t . This run then gives a new $r(t)$ and e_r . From the two resulting simulations one can then extrapolate to zero eccentricity to obtain a more refined tangential momentum parameter. This procedure is illustrated in rows 3, 4, and 5 of table I. In row 3 we have used the $p_t = 8.5013 \times 10^{-2} M$ from Eq. (20) and obtained an eccentricity of 0.004. In row 4 we have increased this p_t by Δp_t which leads to a decrease of the eccentricity to 0.002. A further increase to $p_t = 8.5280 \times 10^{-2} M$ (as in row 5) then yields an eccentricity of 0.0015.

Row 6 of table I shows the initial data that were used to produce Fig. 1. In order to produce an eccentricity which is clearly visible in the $r(t)$ curve we have used a p_t that is deliberately chosen much larger than what is predicted by Eq. (20). In row 7 we show the same configuration (at somewhat closer separation), but this time we choose p_t according to Eq. (20), we see that in this case the eccentricity is already small enough to satisfy e.g. the NRAR guidelines.

In row 8 we have used our method to produce momentum parameters for a similar configuration, but this time both spins point in the negative z -direction. Again we can reach the NRAR target of an eccentricity of order 0.001. In row 9 we also show the eccentricity resulting

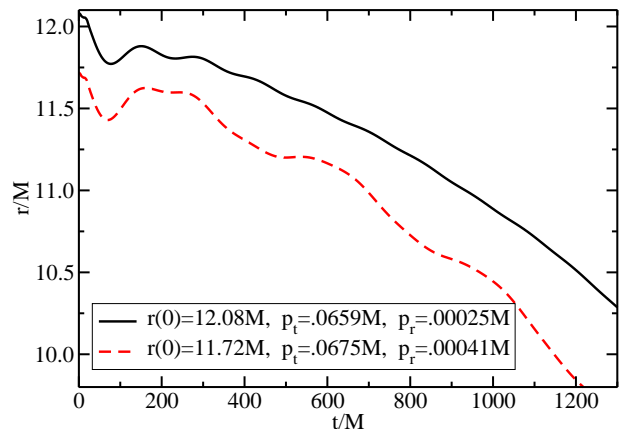


FIG. 3: This plot shows $r(t)$ for the two numerical runs with parameters from rows 8 (solid line) and 9 (broken line) of table I. The parameters for the solid line were picked according to the method explained in this paper while the broken line is the result of setting the parameters according to the much more complicated method in [22]. As we can see the eccentricity difference of about a factor of 5 is quite noticeable in the $r(t)$ curves.

from the method introduced in [22] for the same mass ratio and spin configuration. We can see that it is about 5 times larger, which supports our argument that integrating PN equations of motion does not necessarily lead to better results. The results from these two runs are also shown in Fig. 3. The solid line corresponds to row 8 (i.e. our approach) and the broken line is generated using the approach in [22]. As we can see our method does give a noticeably less eccentric $r(t)$ curve. Notice that the initial dip in the coordinate separation $r(t)$, is due to the aforementioned initial coordinate adjustment. It does not mean the two holes really plunge toward each other initially.

The last five rows of table I give a few more examples of parameters and resulting eccentricities. They show that we can obtain low eccentricities for generic mass ratios and spin orientations.

Notice that our eccentricity reduction method is similar in spirit to the method described in [23, 24], in that we also use short numerical runs to adjust certain parameters. There are, however, important differences. In [23, 24] excision type initial data, not punctures are used. These data are constructed using an extension to the conformal thin sandwich formalism [45]. Empirically it turns out that the tangential momentum that is achieved with the conformal thin sandwich method is quite close to what is needed for low eccentricity data. The main reason for eccentricity is the absence of a radial momentum in the original conformal thin sandwich method. In [23] a method is developed that adds an arbitrary radial velocity parameter to the initial data. This radial velocity parameter together with the tangential momentum are then adjusted to reduce the eccentricity. The method introduced in [23, 24] is capable of producing eccentricities of order of only 10^{-5} . For standard puncture data the method in [23, 24] cannot be used directly. One problem is that standard moving puncture simulations start with the lapse and shift given in Eqs. (18). Thus the coordinates used are not well adapted to quasi-equilibrium. Hence oscillations in the hole separation r are not due to real eccentricity alone but also due to the fact that the coordinates are still evolving as well. This problem is quite visible in Fig. 3. The broken line shows oscillations that have more than one frequency. Thus we cannot fit the curve very well with a straight line plus a single sine function as in [23, 24]. To summarize, reducing the eccentricity for puncture data is harder than for the extended conformal thin sandwich data in [23]. Therefore, our results in both final eccentricities and reduction of eccentricity per iteration are not as good as in [23, 24].

In the cases we have studied so far, we have found it unnecessary to adjust p_r (away from the PN value in Eq. (21)) in order to reach an eccentricity of order 0.001. It is much more important to choose an appropriate p_t . However, we expect that adjusting p_r will be necessary to reach even lower eccentricities.

VI. DISCUSSION

We have introduced the two new eccentricity measures e_r and e_{22} . Both are easy to compute since their calculation does not involve any free parameters unlike earlier definitions akin to $e_\omega(t)$. To compute eccentricity measures such as $e_\omega(t)$ one needs to specify a time interval during the inspiral phase over which we fit the orbital an-

gular velocity to a polynomial of some low degree. This degree is essentially another free parameter and is usually chosen to be 4 or 5. Note, however, that all eccentricity definitions are ambiguous to a certain extent since the entire concept of eccentricity is only rigorously defined for periodic orbits. All eccentricity definitions for inspiral orbits depend on how we split a function of time (like the separation) into a smooth and an oscillating piece. Thus we do not claim that our definitions e_r and e_{22} are less ambiguous than earlier ones. For example our definitions depend on the period T which we compute from Kepler's law, but other choices are possible (e.g. an estimate of the actual orbital period of the numerical simulation at each time). Since our definitions e_r and e_{22} do not require us to choose extra parameters such as fitting intervals they are easier to use.

We also show that certain low resolution grid setups (which are relatively inexpensive) can be used to estimate the initial eccentricity using our measure e_r . This gives us a relatively efficient way to measure the eccentricity of any initial data.

Furthermore, we have explained why the coordinates of standard puncture data are not the same as in PN calculations in ADMTT or harmonic gauge. Thus even if one arrives at a highly accurate estimate of the momentum parameters needed for low eccentricity orbits in ADMTT gauge, there is no easy way to incorporate this knowledge into simulations starting from standard puncture data. Indeed we find that using accurate parameters in ADMTT gauge [21, 22] in standard puncture initial data can lead to relatively large eccentricities.

We provide a simpler approach which starts from momentum parameters using the relatively short expressions given by Kidder [41]. After measuring the resulting eccentricity e_r in a short inexpensive numerical simulation, these parameters can then be refined by changing p_t by an amount of order Δp_t (see Eq. (23)). In this way we can always arrive at eccentricities that are low enough for the purposes of the NRAR collaboration [19]. In order to achieve this we usually do not need more than three numerical runs.

Acknowledgments

It is a pleasure to thank Doreen Müller for useful discussions about the approach in [22]. This work was supported by NSF grant PHY-0855315. Computational resources were provided by the Ranger cluster at the Texas Advanced Computing Center (allocation TG-PHY090095) and the Kraken cluster (allocation TG-PHY100051) at the National Institute for Computational Sciences.

[1] B. Abbott et al. (The LIGO Scientific Collaboration) (2007), arXiv:0711.3041 [gr-qc], 0711.3041.

[2] LIGO, <http://www.ligo.caltech.edu>.

- [3] F. Acernese et al., J. Opt. A: Pure Appl. Opt. **10**, 064009 (2008).
- [4] VIRGO, <http://www.virgo.infn.it>.
- [5] GEO600, <http://www.geo600.org>.
- [6] B. Schutz, Class. Quantum Grav. **16**, A131 (1999).
- [7] T. Nakamura, K. Oohara, and Y. Kojima, Prog. Theor. Phys. Suppl. **90**, 1 (1987).
- [8] M. Shibata and T. Nakamura, Phys. Rev. D **52**, 5428 (1995).
- [9] T. W. Baumgarte and S. L. Shapiro, Phys. Rev. **D59**, 024007 (1998), gr-qc/9810065.
- [10] W. Tichy, Phys. Rev. **D74**, 084005 (2006), gr-qc/0609087.
- [11] W. Tichy, Class. Quant. Grav. **26**, 175018 (2009), 0908.0620.
- [12] W. Tichy, Phys. Rev. **D80**, 104034 (2009), 0911.0973.
- [13] M. Campanelli, C. O. Lousto, P. Marronetti, and Y. Zlochower, Phys. Rev. Lett. **96**, 111101 (2006), gr-qc/0511048.
- [14] J. G. Baker, J. Centrella, D.-I. Choi, M. Koppitz, and J. van Meter, Phys. Rev. Lett. **96**, 111102 (2006), gr-qc/0511103.
- [15] S. Brandt and B. Brügmann, Phys. Rev. Lett. **78**, 3606 (1997), gr-qc/9703066.
- [16] M. Ansorg, B. Brügmann, and W. Tichy, Phys. Rev. **D70**, 064011 (2004), gr-qc/0404056.
- [17] P. C. Peters and J. Mathews, Phys. Rev. **131**, 435 (1963).
- [18] P. C. Peters, Phys. Rev. **136**, B1224 (1964).
- [19] NRAR, <https://www.ninja-project.org/doku.php?id=nrar:home>.
- [20] J. G. Baker, J. R. van Meter, S. T. McWilliams, J. Centrella, and B. J. Kelly, Phys. Rev. Lett. **99**, 181101 (2007), gr-qc/0612024.
- [21] S. Husa, M. Hannam, J. A. Gonzalez, U. Sperhake, and B. Bruegmann, Phys. Rev. **D77**, 044037 (2008), 0706.0904.
- [22] B. Walther, B. Bruegmann, and D. Mueller, Phys. Rev. **D79**, 124040 (2009), 0901.0993.
- [23] H. P. Pfeiffer et al., Class. Quant. Grav. **24**, S59 (2007), gr-qc/0702106.
- [24] M. Boyle, D. A. Brown, L. E. Kidder, A. H. Mroue, H. P. Pfeiffer, M. A. Scheel, G. B. Cook, and S. A. Teukolsky, Phys. Rev. **D76**, 124038 (2007), 0710.0158.
- [25] A. H. Mroue, H. P. Pfeiffer, L. E. Kidder, and S. A. Teukolsky (2010), 1004.4697.
- [26] A. Buonanno, G. B. Cook, and F. Pretorius, Phys. Rev. **D75**, 124018 (2007), gr-qc/0610122.
- [27] B. Brügmann, W. Tichy, and N. Jansen, Phys. Rev. Lett. **92**, 211101 (2004), gr-qc/0312112.
- [28] B. Brügmann, J. González, M. Hannam, S. Husa, U. Sperhake, and W. Tichy, Phys. Rev. **D77**, 024027 (2008), gr-qc/0610128.
- [29] P. Marronetti, W. Tichy, B. Brügmann, J. González, and U. Sperhake, Phys. Rev. **D77**, 064010 (2008), 0709.2160.
- [30] M. J. Berger and J. Olinger, Journal of Computational Physics **53**, 484 (1984).
- [31] T. W. Baumgarte, Phys. Rev. D **62**, 024018 (2000), gr-qc/0004050.
- [32] W. Tichy, B. Brügmann, and P. Laguna, Phys. Rev. **D68**, 064008 (2003), gr-qc/0306020.
- [33] W. Tichy and B. Brügmann, Phys. Rev. D **69**, 024006 (2004), gr-qc/0307027.
- [34] P. Marronetti, W. Tichy, B. Brügmann, J. González, M. Hannam, S. Husa, and U. Sperhake, Class. Quant. Grav. **24**, S43 (2007), gr-qc/0701123.
- [35] B. Brügmann, J. A. González, M. Hannam, S. Husa, U. Sperhake, and W. Tichy, Phys. Rev. **D77**, 024027 (2008), gr-qc/0610128.
- [36] G. Schäfer, Annals of Physics **161**, 81 (1985).
- [37] W. Tichy, B. Brügmann, M. Campanelli, and P. Diener, Phys. Rev. **D67**, 064008 (2003), gr-qc/0207011.
- [38] N. Yunes and W. Tichy, Phys. Rev. **D74**, 064013 (2006), gr-qc/0601046, gr-qc/0601046.
- [39] N. Yunes, W. Tichy, B. J. Owen, and B. Brügmann, Phys. Rev. **D74**, 104011 (2006), gr-qc/0503011.
- [40] N. K. Johnson-McDaniel, N. Yunes, W. Tichy, and B. J. Owen, Phys. Rev. **D80**, 124039 (2009), 0907.0891.
- [41] L. E. Kidder, Phys. Rev. **D52**, 821 (1995), gr-qc/9506022.
- [42] W. Tichy and P. Marronetti, Phys. Rev. **D76**, 061502 (2007), gr-qc/0703075.
- [43] W. Tichy and P. Marronetti, Phys. Rev. **D78**, 081501 (2008), 0807.2985.
- [44] W. Tichy, B. Brügmann, and P. Laguna, Phys. Rev. **D68**, 064008 (2003), gr-qc/0306020.
- [45] J. W. York, Phys. Rev. Lett. **82**, 1350 (1999).
- [46] The standard PN jargon for a term of order $(v/c)^n$ in the equations of motion is $\frac{n}{2}$ PN term. Notice that according to the virial theorem $v^2 \sim M/r$, so that $\frac{n}{2}$ PN terms are also $O(M/r)^{\frac{n}{2}}$.